$$f_L Q^2 = \frac{64 A\mu Q}{\rho D}\left[1+\left(\frac{\mathrm{He} A\mu}{6.2218\rho D}\right)^{0.958}\frac{1}{Q^{0.958}}\right], \quad (31)$$

showing the following equivalence,

$$f_L Q^2 \simeq \frac{64\mathrm{He}^{0.958}\,(A\mu)^{1.958}\,Q^{0.042}}{(6.2218)^{0.958}\,(\rho D)^{1.958}}. \quad (32)$$

From this, and according to equality (28), the expanded expression $f_s Q^2$ is obtained:

$$f_s Q^2 \simeq \frac{64\mathrm{He}^{0.958}\,(A\mu)^{1.958}\,Q^{0.042}}{(6.2218)^{0.958}\,(\rho D)^{1.958}}. \quad (33)$$

IV. Finite-difference equations

This section deals with the numerical discrete method for solving the original partial differential equations. To proceed with the numerical solution, the pipe length is divided into N sub-intervals of equal length Δx as illustrated in Fig. 1. The x domain starts at the pipe entrance $x_1 = 0$ and ends at the exit $x_{N+1} = L$. The variables H and Q are then computed in the discrete domain shown in Fig. 1. Since the physical information are needed from nodes $x_1, x_2, \ldots, x_{N+1}$ to travel along the characteristic lines, a time-step size Δt is computed using following formula:

$$\Delta t = C_r \frac{\Delta x}{a}, \quad (34)$$

where the Courant number C_r must be less than or equal to 1 [25]:

$$C_r \leq 1. \quad (35)$$

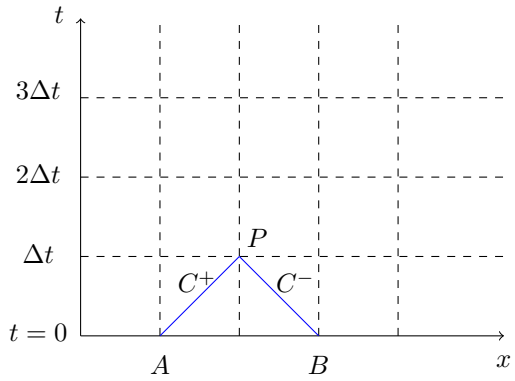

Fig. 1: Numerical characteristics grid lines on the xt plane.

Thus, the size of Δx and the wave celerity a (see (2), (3), (6), (7)) determine the size of our time interval. Defining the characteristic lines C^+ and C^- respectively by lines AP and BP, given previously by (13) and (15). Next, assuming that the variables H and Q are known at points A and B. The aim here is to know these variables at point P. For that, the integration method between these points solves equations (13) and (15) with regard to H and Q:

$$H_{P_i} = \frac{1}{2}\Big[(H_{i-1}+H_{i+1}) + B(Q_{i-1}-Q_{i+1}) + R_{i+1}Q_{i+1}|Q_{i+1}| - R_{i-1}Q_{i-1}|Q_{i-1}|\Big]. \quad (36)$$

$$Q_{P_i} = \frac{1}{2B}\Big[(H_{i-1}-H_{i+1}) + B(Q_{i-1}+Q_{i+1}) - R_{i+1}Q_{i+1}|Q_{i+1}| - R_{i-1}Q_{i-1}|Q_{i-1}|\Big]. \quad (37)$$

In which, B is the Allievi constant, R_A and R_B are the resistance coefficients called the radius of gyration defined respectively at points A and B, which are given by:

$$B = \frac{a}{gA}, R_A = \frac{f_A \Delta x}{2gDA^2}, R_B = \frac{f_B \Delta x}{2gDA^2}. \quad (38)$$

The stability analysis takes a huge role in numerical schemes allowing to perform this model problem. Hence, the stable solution should be smaller than a certain critical value. The numerical stability is developed using Von Neumann analysis, satisfying inequality (35). In which, the Courant number C_r is given by:

$$C_r = \frac{f\Delta Q \Delta t}{4DA}. \quad (39)$$

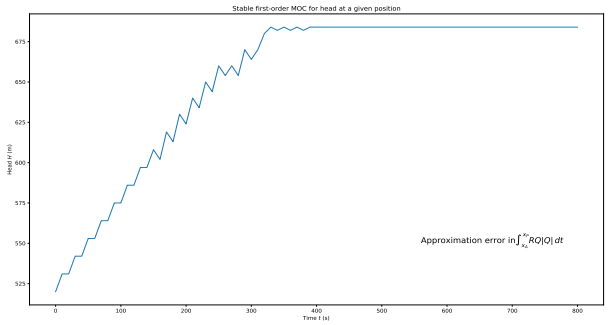

Fig. 2: Stable first-order MOC for head at a given position.

The authors in [26] investigate the numerical stability and accuracy of the MOC method by analyzing typical piping systems with some parameters and empirical stability limits. They studied predictor-corrector procedure. First, predict values for head-discharge are used to obtain secondly a corrected values, limiting consequently time computation. Noticing that if friction loss term is supposed large, then finite-difference scheme is unstable even if inequality (35) is satisfied. They establish the following stability criterion. When the Courant condition C_r value is less than 0.5, the first-order approximation yields stable results. This approximation works well while

the friction term is small. Further, a second-order method of characteristics is conditionally stable for C_r value lower than 0.79, i.e. $C_r \leq .79$. In order to illustrate this stability for $C_r \leq 0.5$ using first-order MOC. Fig. 2 reports that head H reaches its peak that its maximum is near to attempt exact value.

V. Stationary solutions

The aim here is to determine the steady fluid flow. We give an explicit analytic representation of the stationary solutions of equations (10) and (12), and compare with the approximated solutions which are illustrated by the numerical simulations. The stationary solution still can be computed explicitly. Finally, we study the goodness of the approximations using the perturbation techniques.

A. Initial and boundary conditions

Boundary conditions (see Fig. 3) are essentially a relationship between head H and discharge Q at a boundary node, which can then be solved with the characteristic equations to provide a full solution for the boundary. In the models the head-discharge relationship at the boundary can often be solved simultaneously with the appropriate characteristic equations to produce a direct solution. Each boundary condition is solved independently of the other boundary, and independently of the interior point.

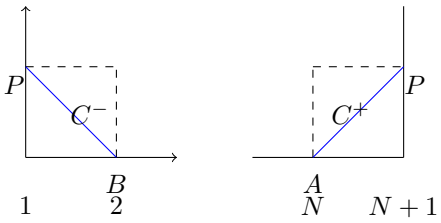

Fig. 3: Characteristics at boundaries.

We use Dirichlet boundary condition to get the stationary solutions. We impose at the upstream and downstream ends the same value of discharge Q_0 that reads as:

$$Q(x_{N+1}) = Q(x_1) = Q_0. \tag{40}$$

We recall that $x_1, x_2, \ldots, x_{N+1}$ are the nodes of the physical domain. Denoting the upstream boundary head $H(t_1, x_1)$ by $H(x_1)$, and the downstream boundary head $H(t_1, x_{N+1})$ by $H(x_{N+1})$. The quantity $H(x_{N+1})$ is expressed in terms of $H(x_1)$:

$$H(x_{N+1}) = H(x_1) - \frac{fLQ|Q|}{2gDA^2}. \tag{41}$$

Initializing the head H with constant $H(x_1)$, meaning that:

$$\forall i \in [\![1; N+1]\!], H_0(x_i) = H(x_1). \tag{42}$$

The initial discharge is defined by constant Q_0:

$$\forall i \in [\![1; N+1]\!], Q_0(x_i) = Q_0. \tag{43}$$

B. Exact solutions

Consider a fluid entering a circular pipe presented in Fig. 4. A stationary state of the model is constituted by the conservative variables H and Q that remain in the same state. According to equation (10), if the head H is independent of time, then the discharge Q is constant in space. Otherwise, the discharge Q does not vary over time, the discharge Q is constant in space and time. In the steady-state, the discharge Q is equal to constant Q_0:

$$Q(t, x) = Q_0. \tag{44}$$

From this, equation (12) yields:

$$\frac{\partial H}{\partial x} = -\frac{fQ|Q|}{2gDA^2}, \tag{45}$$

which is coupled with equality (44) to get:

$$\frac{\partial H}{\partial x} = -\frac{fQ_0|Q_0|}{2gDA^2}. \tag{46}$$

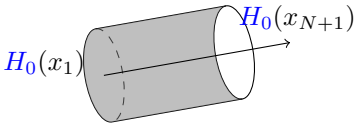

Fig. 4: The flow of a fluid in a circular pipe.

We notice that the friction f depends on the discharge Q which is a constant. By integrating equation (45) between inferior bound x_1 and superior bound x, we get:

$$H(t, x) = H(x_1) - \frac{fQ_0|Q_0|}{2gDA^2}(x - x_1). \tag{47}$$

Equation (47) implies that the head H is an affine function of a decreasing slope. It can be given in the discrete form:

$$\forall i \in [\![2; N]\!], H(x_i) = H(x_1) - \frac{fQ_0|Q_0|}{2gDA^2}(x_i - x_1). \tag{48}$$

We present the numerical results in Figs. 5-6 that are shared into five pictures. Fig. 5 shows the evolution of head over space in the stationary state.

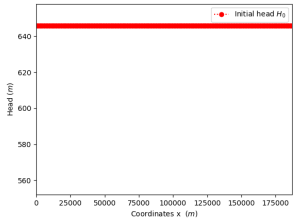

(a) Initial head $H_0(x)$.

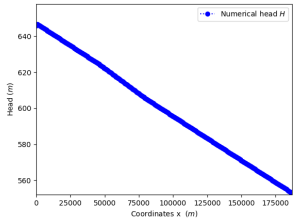

(b) Head $H(t, x)$ at $T_{\max}$.

Fig. 5: Evolution of head over space in steady-state.

The initial head H_0 is presented in picture 5a. The head generated by the numerical code using the method of characteristics is the same that is the exact one given by equality (47). It is concluded that these results are consistent with the model. Initializing discharge in 6a with the value Q_0. At the final stage of time, the numerical discharge Q is shown in picture 6b. The slant of view of this simulation is interpreted as follows. The discharge Q remains in the same state as time elapses, in every observable instant. This means that it is unchanging in time. Indeed, this discharge Q is equal to the constant Q_0 (see equality (44)). Now, setting a scale with precision near from 10^{-15}, the numerical oscillations appear, meaning of numerical noises. This discharge Q is presented in picture 6c. Consequently, the steady-state is approached asymptotically, proving that state variables are unchanging in continuous time.

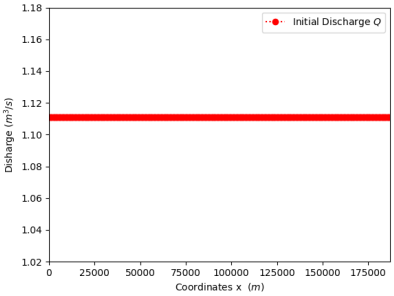

(a) Initial discharge $Q_0(x)$.

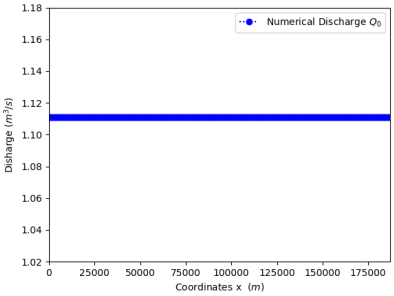

(b) Discharge $Q(t,x)$ at $T_{\max}$.

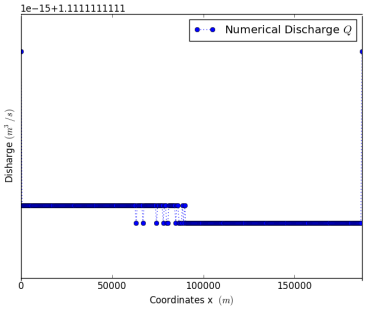

(c) Numerical discharge $Q(t,x)$ at $T_{\max}$ with precision.

Fig. 6: Evolution of discharge over space in steady-state.

VI. Instationary solutions

This section essentially deals with the so-called three-fluid model. In this model, we focus on the study the instationary flow. The pipeline is divided into three sections as shown in Fig. 7. Consider a water streaming the first section which is defined between two points x_1 and x_{N_1+1}. Next, the slurry flows in the second one $[x_{N_1+1}, x_{N_2+1}]$. The water dominates the third section $]x_{N_2+1}, x_{N+1}]$ allowing the slurry to exit from the pipeline. We assume that there is no direct contact between water and slurry. The first water domain is subdivided into a finite number N_1 of cells. These cells cover entirely this computational domain. Similarly, $N_2 - N_1$ means the number of slurry cells that we will give its value later.

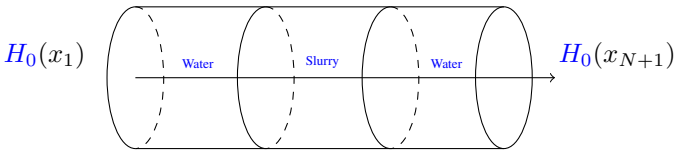

Fig. 7: Schematics of water-slurry-water flow in a circular pipe.

It is necessary to know the initial conditions in order to be able to set the system of equations (10) and (12). Initialise this state involves running the head-discharge over time using equalities (36) and (37). It leads to determine the pressure drop in next discrete step knowing its previous value in time. A shift in the elevation start takes place, meaning that water begins to flow above slurry. The target of this shifted hydraulic head is to cause the unsteady state in the system. We assume in this case a constant rate Q_0 for the initial discharge Q_0^i:

$$Q_0^i(x) = Q_0, \tag{49}$$

and the initial head H_0^i is obtained by following equality:

$$H_0^i(x) = \begin{cases} H(x_1) - \frac{f_w Q_0 |Q_0|}{2gDA^2}(x - x_1),\ x \in [x_1, x_{N_1+1}], \\ H(x_1) - \frac{f_s Q_0 |Q_0|}{2gDA^2}(x - x_1),\ x \in]x_{N_1+1}, x_{N_2+1}], \\ H(x_1) - \frac{f_w Q_0 |Q_0|}{2gDA^2}(x - x_1),\ x \in]x_{N_2+1}, x_{N+1}], \end{cases} \tag{50}$$

in which f_w and f_s are the friction factors for water and slurry, which are computed according to equalities (21) and (27), respectively. The speeds of sound in water and slurry are given by quantities a_w and a_s, which are computed using equalities (2) and (6), respectively.

The nature of boundary conditions used here is explained as follows. We apply the Dirichlet boundary conditions for the variable H. It means that $H(x_1)$ corresponds to the value of head H at the inlet. The relation between the head H at the upstream boundary $H(x_1)$, and at the downstream boundary $H(x_{N+1})$ is given by the following equality:

$$H(x_{N+1}) = H(x_1) - \frac{f_w L Q_0 |Q_0|}{2gDA^2}. \quad (51)$$

For the discharge Q, the Neumann condition is imposed at the upstream boundary while the Dirichlet condition is adjusted at the downstream boundary.

In the remainder of this paper, we set the distance 47000 meters of the node x_{N_1+1} in where the slurry begins to travel. Setting the position x_{N_2+1} at where the interface of slurry ends to value 80000 meters. The discrete number of slurry cells is given by:

$$N_2 - N_1 = \left\lfloor \frac{x_{N_2+1}}{\Delta x} \right\rfloor - \left\lfloor \frac{x_{N_1+1}}{\Delta x} \right\rfloor. \quad (52)$$

For our numerical setup, the slurry grid size is 10^4, i.e.

$$N_2 - N_1 = 10^4. \quad (53)$$

In what follows, we detail here how the interface slurry-water is solved. There are any restrictions for treating the interface linking the water and slurry, and conversely. For instance, ghost cells are not used to close the computational interfaces. The initial interface water-slurry is physically discontinuous in nature. The value at this interface is defined as the averaged value of left and right limits that is updated at each discrete-time. Consequently, the ended water cell influences the beginning slurry cell which comes after it. Similarly, the last slurry node effects the starting water node.

We know that the experimental results are essential to be compared with the numerical ones. However, these information are purposely censored because, for many confidentiality reasons. The missing data will not affect the fitting of the model because it will be validated numerically with only interpretation. In addition, the properties of the used fluids are shown bellow by table I.

TABLE I: General input datas describing parameters and their values used in model.

Physical variables	Numerical values	Dimensions
Pipe length, L	187.10^3	m
Diameter of pipe, D	0.9	m
Wall thickness of pipe, e	0.017	m
Density of water, ρ_w	10^3	kg/m^3
Dynamic viscosity of water, μ_w	10^{-3}	$Pa.s$
Wave speed of water, a_w	1037.57	m/s
Elastic modulus of water, K_w	$2.19.10^9$	GPa or N/m^2
Density of slurry, ρ_s	1600	kg/m^3
Dynamic viscosity of slurry, μ_s	0.0102	$Pa.s$
Wave speed of slurry, a_s	971.34	m/s
Elastic modulus of phosphate, K_f	8.10^{10}	GPa or N/m^2
Young modulus, E	112.10^9	N/m^2
Final time, $T_{\max}$	252	s
Concentration of solid phase, C_s	0.4	dimensionless

Six targeted flashed images are illustrated in Fig. 8 to simulate the unsteady-state of three-fluid flow. This head H_0 defined by equality (50) is shown in picture 8a. This initial head H_0 is a discontinuous function due to water's density being less than liquid slurry's. This comparison is justified by using equality (21). It is concluded that the friction coefficient f_w is less than the slurry one f_s, showing that the hydraulic-grade-line elevation for slurry is under water.

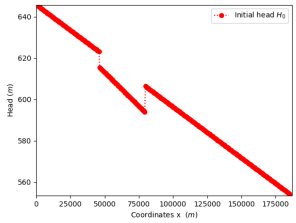

(a) Initial head $H_0(x)$.

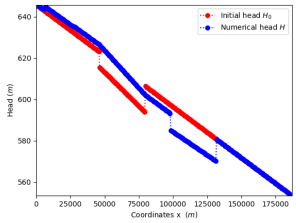

(b) $H_0(x)$ and numerical head $H(84, x)$.

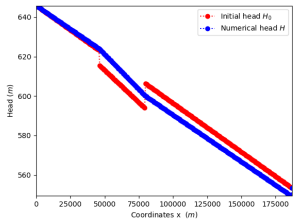

(c) Head $H(t, x)$ at $T_{\max}$ compared to H_0.

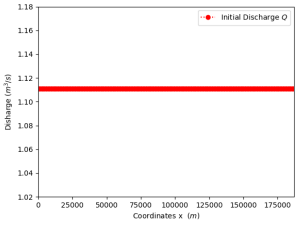

(d) Initial discharge $Q_0(x)$.

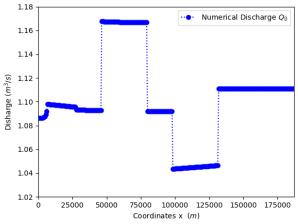

(e) Discharge $Q(t, x)$ at instant 84.

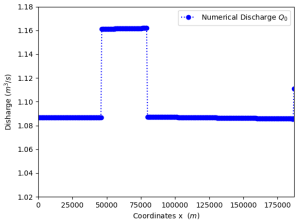

(f) Discharge $Q(t, x)$ at $T_{\max}$.

Fig. 8: Evolution of head-discharge over space in unsteady-state.

The interpretation of the simulation defined in pictures 8b and 8c are given as follows. The flow is shared into two parts. The first one L_1 is constituted with left water and slurry. The mixture of these two liquids forms one having an elevation which is close to slurry one. This liquid goes to the left side and reflects. The second one L_2 is constituted with slurry and right water. The fluid's particles generated by this mixture move over the pipeline. At time 84, the interaction between liquids L_1 and L_2 give fluid's particles that are ready to leave the right side. Insisting here that instant 84 is given by $T_{\max}$ per 3, and it is valid in the rest of the paper. This instant means occurring the move forward of slurry from middle section to the next one. Showing its transport is important in modeling framework. The picture 8c shows that these particles exit the pipeline at instant $T_{\max}$. Only one mixture of liquids L_1 and L_2 dominates the flow generating one fluid at the final time.

Now, we give how the discharge varies in pictures 8d, 8e and 8f. Setting the initial discharge Q_0 to value $\frac{10}{9}$, i.e. $Q_0 =$

$\frac{10}{9}$. This discharge Q_0 defined by equality (49) is shown in picture 8d, meaning that is constant at initial time in terms of position's pipeline. In the beginning of this simulation, the discharge is ever constant in the second region. It follows that at instant 84, the moving slurry's discharge is less than the water one (see picture 8e). The model converges to a piecewise function presented in picture 8f. It is allowing to generate the same discharge in the first and last regions, and greater one in the middle region.

Consequently, these researches given by pictures 6 and 8 focused on predicting pressure drop and discharge in cement slurry flow in circular pipe. Results showed that regime unsteady-state determine only one state in the final stage. This slurry was produced over time with mixing phosphate and water. When convergence time occurs, the final state shows that the head is homogeneous. Since single-phase fluid is pipelined at large distances, slurry particles are concentrated on the bottom of the pipeline. At instant $T_{\max}$, this mixture exit from the pipe. Regarding discharge Q, it is the same one at inlet and outlet sections, even it is a discontinuous function in space.

VII. Coupling Models

In this section, we keep the same modeling introduced previously in section VI as shown in Fig. 9. We are interested in transport of three-fluid through a pipeline in unsteady-state. Here, three artificial conditions are imposed at each part of sections. In this model, the fluid flow in each section does not impact the other one. It means that the flow is not transmitted from one section to another one. There is any influence between slurry and water. To develop this model, equations (10) and (12) must be solved together in each section of the pipeline independently on other. These equations are solved using the method of characteristics. Noticing that this model does not reflect the physical reality. However, it is built in order to be converged at final time to the steady-state.

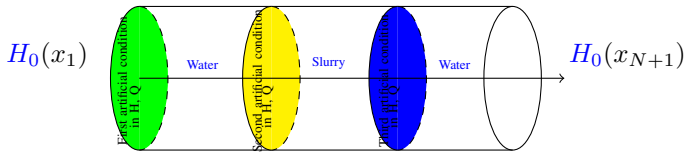

Fig. 9: Schematics of water-slurry-water flow in a circular pipe with artificial conditions.

The initial discharge Q_0^i is defined in terms of two constants Q_0 and Q_1:

$$Q_0^i(x) = \begin{cases} Q_0,\ x \in [x_1, x_{N_1+1}], \\ Q_1,\ x \in]x_{N_1+1}, x_{N_2+1}], \\ Q_0,\ x \in]x_{N_2+1}, x_{N+1}], \end{cases} \tag{54}$$

and the initial head H_0^i is given by:

$$H_0^i(x) = \begin{cases} H(x_1),\ x \in [x_1, x_{N_1+1}], \\ H(x_1) - \frac{f_s Q_1 |Q_1|}{2gDA^2}(x_{N_1+1} - x_1),\ x \in]x_{N_1+1}, x_{N_2+1}], \\ H(x_1) - \frac{f_w Q_0 |Q_0|}{2gDA^2}(x_{N_2+1} - x_1),\ x \in]x_{N_2+1}, x_{N+1}]. \end{cases} \tag{55}$$

We will apply the Dirichlet boundary conditions for the head H at the upstream boundary of each section. These upstream boundaries are given by quantities $H(x_1)$, $H(x_{N_1+1})$, and $H(x_{N_2+1})$ which are defined respectively by:

$$H(x_1) = H_0^i(x_1). \tag{56}$$

$$H(x_{N_1+1}) = H(x_1) - \frac{f_s Q_1 |Q_1|}{2gDA^2}(x_{N_1+1} - x_1). \tag{57}$$

$$H(x_{N_2+1}) = H(x_1) - \frac{f_w Q_1 |Q_1|}{2gDA^2}(x_{N_2+1} - x_1). \tag{58}$$

The head at the downstream boundary is defined by the Neumann condition at each parts of section. In what to follow, for the discharge Q, we impose the Neumann condition at the upstream boundary. On the contrary, the Dirichlet condition is adjusted at the downstream boundary.

The variation of head-discharge is shown in Fig. 10 that is shared into two pictures, given below:

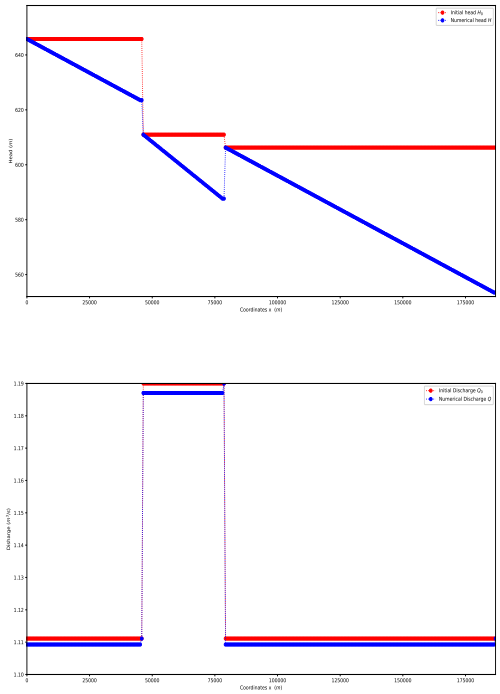

Fig. 10: Coupling models and evolution of head-discharge over space in unsteady-state.

The initial head H_0 defined by equality (55) is shown in the top picture. This head is a piecewise constant function, which is equal to $H(x_1)$ over the first region, to $H(x_1) - \frac{f_s Q_1|Q_1|}{2gDA^2}(x_{N_1+1} - x_1)$ between positions x_{N_1+1} and x_{N_2+1} and to $H(x_1) - \frac{f_w Q_0|Q_0|}{2gDA^2}(x_{N_2+1} - x_1)$ over the last region. The discharge is initialized according to equality (54), that is shown in the bottom picture, and its evolution until instant $T_{\max}$ is presented in the same picture. The head converges to a piecewise affine function when time goes to the final instant $T_{\max}$. This elevation of the three-fluid model is not the same, showing that the fluid is not homogeneous due to utilization of three different artificial conditions. Noticing that we showed in section V that each component head converges to affine function with a decreasing slope. In the same case the discharge remains the same. The same reasoning is available for head-discharge constituting each piece, justifying this result. It is concluded that the unsteady flow converges to the steady-state, achieving the validation of this model.

VIII. Conclusion

The slurry transportation has been mainly studied and it is shown that the flow is stable in presence of water. In summary, we have applied the method of characteristics for compressible multi-fluid flow which is described by hyperbolic systems. We have tested over this paper the ability of the code to conserve the pipeline in steady-state. We have shown also the results that regime unsteady-state determine the solution in different time durations. Additionally, the numerical results were analyzed based on various flow conditions. In the future, we would like to extend the numerical code for the simulation to higher dimensions, and generalize it particularly to three-dimensional problems fairly easily. On the other hand, even the method of characteristics is efficient compared to the finite volume method [27], and it is capable of the advantages of high accuracy. Moreover, numerical tests will be performed by comparing results of these two numerical methods. To analyze two-phase flow under the influence of various floating particles, it is necessary to develop a new model which investigates the mechanism of their interaction. A few recent works have proposed this study [28], [29], [30]-[31]. On others words, establishing the multiphase model with considering solid-liquid two-phase coupling, as mentioned in [32]. It is observed that computational fluid dynamics (CFD) modeling gives fairly good results to simulate the slurry flow in pipeline [33], [34]. It is interesting to use CFD calculations by using Eulerian model and compare it with the developed one.

Acknowledgment

I would like to thank the anonymous reviewers for their helpful comments and valuable suggestions to improve quality of this article. This work was supported by the research federation Math-STIC, University Paris 13.

References

[1] A. Mackenzie, M. T. SticklandW and M. Dempster, "Development of a Combined Euler-Euler Euler-Lagrange Slurry Model," *OpenFOAM®*, pp. 77-91, 2019.

[2] M. H. Kasbaoui, D. L. Koch and O. Desjardins, "Clustering in Euler–Euler and Euler-Lagrange simulations of unbounded homogeneous particle-laden shear," *Journal of Fluid Mechanics*, vol. 859, pp. 174-203, 2019.

[3] S. A. Miedema, "A head loss model for homogeneous slurry transport for medium sized particles," *Journal of Hydrology and Hydromechanics*, vol. 63, no. 1, pp. 1-12, 2015.

[4] F. Benkhaldoun, I. Elmahi and M. Seaı, "Well-balanced finite volume schemes for pollutant transport by shallow water equations on unstructured meshes," *Journal of computational physics*, vol. 226, no. 1, pp. 180-203, 2007.

[5] T. Chakkour, "Simulations numériques des tubes avec contraction brusque sur openfoam," *Thermodynamique des interfaces et mécanique des fluides*, vol. 17, no. 1, 2017.

[6] M. Ishii and K. Mishima, "Two-fluid model and hydrodynamic constitutive relations," *Nuclear Engineering and design*, vol. 82, no. 2-3, pp. 107-126, 1984.

[7] J. Wang, S. Wang, T. Zhang and F. Battaglia, "Mathematical and experimental investigation on pressure drop of heterogeneous ice slurry flow in horizontal pipes," *International Journal of Heat and Mass Transfer*, vol. 108, pp. 2381-2392, 2017.

[8] G. Shou, *Slurry pipeline system: Simulation and validation*

[9] J. Rusconia, A. Lakhouajab, and M. Kopuzc, "The Design and Engineering of the 187 km Khouribga to Jorf Lasfar Phosphate Slurry Pipeline," *Procedia Engineering*, vol. 138, pp. 142-150, 2016.

[10] B. Geissler, L. Hermann, M. C. Mew and G. Steiner, "Striving toward a circular economy for phosphorus: the role of phosphate rock mining," *Minerals*, vol. 8, no. 9, pp. 395-417, 2018.

[11] S. Yao, Y. Li, W. Wang, G. Song, Z. Shi, X. Wang, and S. Liu, "Investigation of hydrate slurry flow behaviors in deep-sea pipes with different inclination angles," *Oil & Gas Science and Technology–Revue d'IFP Energies nouvelles*, vol. 74, pp. 48-60, 2019.

[12] B. Shi, Y. Liu, L. Ding, X. Lv, J. Gong, "New Simulator for Gas–Hydrate Slurry Stratified Flow Based on the Hydrate Kinetic Growth Model," *Journal of Energy Resources Technology*, vol. 141, no. 1, 2019.

[13] D. J. Wood and T. Y. Kao, "Unsteady flow of solid-liquid suspensions," *Journal of the Engineering Mechanics Division*, vol. 92, no. 6, pp. 117-134, 1966.

[14] W. Bechteler and G. Vogel, "Pressure wave velocity in slurry pipelines," *Proceedings of Hydrotransport*, vol. 8, 1982.

[15] ARD. Thorley and L. Y. Hwang, "Effects of rapid change in flowrate of solid-liquid mixtures," *Proceedings of Hydrotransport 6th Conference, UK*, pp. 229-242, 1979.

[16] E. B. Wylie, V. L. Streeter and L. Suo, "Fluid transients in systems," *Prentice Hall Englewood Cliffs*, vol. 1, 1993.

[17] E. B. Wylie and V. L. Streeter, "Fluid transients," *New York, McGraw-Hill International Book Co.*, 1978.

[18] M. Grozdek, R. Khodabandeh and P. Lundqvist, "Experimental investigation of ice slurry flow pressure drop in horizontal tubes," *Experimental Thermal and Fluid Science*, vol. 33, no. 2, pp. 357-370, 2009.

[19] J. T. Park, R. J. Mannheimer, T. A. Grimley, and T. B. Morrow, "Pipe flow measurements of a transparent non-newtonian slurry," *Journal of fluids engineering*, vol. 111, no. 3, pp. 331-336, 1989.

[20] R. W. Hanks and B. H. Dadia, "Theoretical analysis of the turbulent flow of non-newtonian slurries in pipes," *AIChE Journal*, 1971.

[21] R. Darby and J. Melson, "How to predict the friction factor for flow of bingham plastics," *Chemical Engineering*, vol. 88, no. 26, pp. 59-61, 1981.

[22] R. Darby, R. Mun and D. V. Boger, "Predict friction loss in slurry pipes," *Chemical Engineering*, vol. 99, no. 9, pp. 116-119, 1992.

[23] E. Buckingham, "On plastic flow through capillary tubes," *Proceedings-American society for testing and materials*, pp. 1154-1156, 1921.

[24] S. W. Churchill, "Friction-factor equation spans all fluid-flow regimes," *Chemical engineering*, vol. 84, no. 24, pp. 91-92, 1977.

[25] R. J. Fennema and M. H. Chaudhry, "Explicit numerical schemes for unsteady free-surface flows with shocks," *Water Resources Research*, vol. 22, no. 13, pp. 1923-1930, 1986.

[26] M. B. Holloway and M. H. Chaudhry, "Stability and accuracy of waterhammer analysis," *Advances in Water Resources*, vol. 8, 1985.

[27] R. Liu, D. Wang, X. Zhang, W. Li, and B. Yu, "Comparison Study on the Performances of Finite Volume Method and Finite Difference Method," *Journal of Applied Mathematics*, vol. 2013, 2013.

[28] Y. H. Song, E. H. Lee and J. H. Lee, "Functional relationship between soil slurry transfer and deposition in urban sewer conduits," *Water*, vol. 10, no. 7, pp. 825-841, 2018.

[29] S. Akhtar, H. Ali and C. W. Park, "Thermo-Fluidic Characteristics of Two-Phase Ice Slurry Flows Based on Comparative Numerical Methods," *Processes*, vol. 7, no. 12, pp. 898-914, 2019.
[30] A. Amani, N. Balcázar, A. Naseri, J. Rigola, "A numerical approach for non-Newtonian two-phase flows using a conservative level-set method," *Chemical Engineering Journal*, vol. 385, pp. 123896-123916, 2020.
[31] T. Chakkour, "Application of two-dimensional finite volume method to protoplanetary disks," *Astronomy Letters*, under review, 2020.
[32] X. J. Shi and P. Zhang, "Two-phase flow and heat transfer characteristics of tetra-n-butyl ammonium bromide clathrate hydrate slurry in horizontal 90° elbow pipe and U-pipe," *International Journal of Heat and Mass Transfer*, vol. 97, pp. 364-378, 2016.
[33] O. Parkash, A. Kumar, B. S. Sikarwar, "CFD Modeling of Commercial Slurry Flow Through Horizontal Pipeline," *Advances in Interdisciplinary Engineering*, pp. 153-162, 2019.
[34] A. Kumar, "CFD Modeling for Slurry Flow Through Bends and Straight Pipe Line," *CAD/CAM, Robotics and Factories of the Future*, pp. 615-623, 2016.
[35] C. Tao, B. G. Kutchko, E. Rosenbaum and M. Massoudi, "A Review of Rheological Modeling of Cement Slurry in Oil Well Applications," *Energies*, vol. 13, no. 3, pp. 570-622, 2019.
[36] N. Kumar, M. K. Gopaliya, D. R. Kaushal, "Experimental investigations and CFD modeling for flow of highly concentrated iron ore slurry through horizontal pipeline," *Particulate Science and Technology*, vol. 37, no. 2, pp. 232-250, 2019.
[37] T. Chakkour, "Some notes about the continuous-in-time financial model," *Abstract and Applied Analysis*, vol.2017, 2017, Hindawi.
[38] T. Chakkour, "Inverse problem stability of a continuous-in-time financial model," *Acta Mathematica Scientia*, vol. 39, no. 5, pp. 1423-1439, 2019.
[39] G.Camera-Roda, V.Augugliaro, A. G. Cardillo, V.Loddo, L. Palmisano, F.Parrino, F.Santarelli, "A reaction engineering approach to kinetic analysis of photocatalytic reactions in slurry systems," *Catalysis Today*, vol. 259, pp. 87-96, 2016.
[40] N. Kumar, M. K. Gopaliya and D. R. Kaushal, "Experimental investigations and CFD modeling for flow of highly concentrated iron ore slurry through horizontal pipeline," *Particulate Science and Technology*, vol. 37, no. 2, pp. 232-250, 2019.
[41] J. R. Januário and C. B. Maia, "CFD-DEM simulation to predict the critical velocity of slurry flows," *Journal of Applied Fluid Mechanics*, vol. 13, no. 1, pp. 161-168, 2020.
[42] G. M. Oliveira and A. T. Franco, "Mathematical Model for Viscoplastic Fluid Hammer," *Journal of Fluids Engineering*, vol. 138, no. 1, 2016.
[43] N. Ijaz, A. Zeeshan, M. M. Bhatti, R. Ellahi, "Analytical study on liquid-solid particles interaction in the presence of heat and mass transfer through a wavy channel," *Journal of Molecular Liquids*, vol. 250, pp. 80-87, 2018.